Alexandria Engineering Journal (2015) xxx, xxx–xxx

HOSTED BY

Alexandria University

Alexandria Engineering Journal

www.elsevier.com/locate/aej
www.sciencedirect.com

ORIGINAL ARTICLE

Three dimensional boundary layer flow of a viscoelastic nanofluid with Soret and Dufour effects

M. Ramzan [a,*], Saba Inam [b], S. A. Shehzad [c]

[a] Department of Mathematics, College of Science, Al-Zulfi, Majmaah University, Saudi Arabia
[b] Department of Mathematics, Faculty of Computing, Mohammad Ali Jinnah University, Islamabad Campus, Pakistan
[c] Department of Mathematics, Comsats Institute of Information Technology, Sahiwal 57000, Pakistan

Received 9 June 2015; revised 13 September 2015; accepted 29 September 2015

KEYWORDS

Soret Dufour effects;
Viscoelastic fluid;
Nanoparticles;
Nonlinear analysis

Abstract The present research focuses on the three-dimensional flow of viscoelastic fluid in the presence of Soret and Dufour effects. Effects of thermophoresis and Brownian motion are taken into account. Appropriate similarity transformations lead to nonlinear ordinary differential equations. Solution expressions of velocity, temperature and nanoparticle concentration are computed via homotopy analysis method (HAM). Convergence of obtained solutions is analyzed graphically and numerically. Results are plotted and analyzed for the dimensionless velocities, temperature and nanoparticle concentration. Values of local Nusselt and Sherwood numbers are examined through tabular form. It is observed that Temperature field is enhanced for the larger Brownian motion parameter and an increase in Dufour number gives rise to the temperature and thermal boundary layer thickness.

1. Introduction

Heat transfer mechanism has an important role in many engineering and industrial fields because cooling and heating processes are involved in such fields. An increase in heat transfer rate is quite essential. It reduces the process time of work and length of the work life of equipment. Various methods are proposed in the past to increase the heat transfer efficiency rate. Some methods involve extended surfaces, applications of vibration to the heat transfer surfaces and usage of micro-channels is studied by Kwak and Kim [1]. There is another method to increase the heat transfer efficiency by increasing the thermal conductivity of the working fluids as mentioned by Ramzan [2]. Most commonly used working fluids such as water, engine oil, and ethylene glycol have lower thermal conductivity compared to the thermal conductivity of solids. Solids of higher thermal conductivity can be utilized to increase the thermal conductivity of the base fluid by emerging small solid particles in the fluid. Emerging of such particles in the base fluid is known as nanofluid. Such fluids have several applications in biomedical and engineering applications in cooling, cancer therapy and process industries. A tremendous work on nanofluids can be seen in Refs. [3–12].

The boundary layer flow over a continuously stretching surface is commonly encountered in various industrial and

* Corresponding author.
E-mail address: m.ramzan@mu.edu.sa (M. Ramzan).
Peer review under responsibility of Faculty of Engineering, Alexandria University.

http://dx.doi.org/10.1016/j.aej.2015.09.012
1110-0168 © 2015 Faculty of Engineering, Alexandria University. Production and hosting by Elsevier B.V.

engineering processes such as materials manufactured by extrusion of plastic sheets and materials traveling between a windup roll and feed roll. Numerous studies have been done on the two-dimensional boundary layer flow over a stretching surface. Not much attention is paid to three-dimensional boundary layer flow induced by stretching surface. Wang [13] was the first who investigated the three-dimensional boundary layer flow of viscous fluid over a bidirectional stretching surface and provided exact solution. Later on Ariel [14] constructed the homotopy perturbation solution of Wang [13] flow problem. Hayat et al. [15] computed the series solutions of three-dimensional of an Oldroyd-B fluid in the presence of convective boundary conditions. Hydromagnetic flow of Maxwell fluid induced by a bidirectional stretching surface with variable thermal conditions is investigated by Shehzad et al. [16]. Ahmad et al. [17] studied the hydromagnetic flow of three-dimensional viscous fluid in the presence of heat generation/absorption. Some useful studies may be found through [18–20].

In all the abovementioned studies, the influences of Soret and Dufour effects are not addressed because they have smaller order of magnitude than the effects described by Fourier's and Fick's laws. Eckert and Drake [21] investigated that there are several cases where such effects cannot be neglected. Soret and Dufour effects are important for the fluids which have light molecular weight or medium molecular weight. Turkyilmazoglu and Pop [22] discussed the Soret and heat source effects on unsteady radiative flow of viscous fluid induced by an impulsively started infinite vertical plate. Combined effects of partial slip, thermal diffusion and diffusion thermo, in steady flow of viscous fluid generated by a rotating disk were examined by Rashidi et al. [23]. Alsaedi et al. [24] analyzed the Soret and Dufour effects on two-dimensional boundary layer flow of second grade fluid over a stretching surface. Stagnation point flow of Jeffery fluid induced by a convectively heated sheet under Soret and Dufour effects is addressed by Shehzad et al. [25].

The aim of the present work is to study the effects of Soret and Dufour on the boundary layer flow of viscoelastic fluid in the presence of nanoparticles and chemical reaction. No such analysis is provided in the literature. We used homotopy analysis method (HAM) [26–33] to discuss the solution of velocities, temperature and nanoparticle concentration. The heat transfer rate and nanoparticles concentration transfer rate at the walls are computed numerically.

2. Mathematical formulation

We consider the three-dimensional flow of an incompressible viscoelastic nanofluid over a stretching surface at $z=0$. The motion in fluid is induced due to the stretching of surface. The heat and nanoparticle mass transfer characteristics have been considered when both Soret and Dufour effects are present. The continuity, momentum, energy and nanoparticle concentration equations for the boundary layer flow are given below:

$$\frac{\partial u}{\partial x}+\frac{\partial v}{\partial y}+\frac{\partial w}{\partial z}=0, \tag{1}$$

$$u\frac{\partial u}{\partial x}+v\frac{\partial u}{\partial y}+w\frac{\partial u}{\partial z}=v\frac{\partial^2 u}{\partial z^2}-K\left(u\frac{\partial^3 u}{\partial x\partial z^2}+w\frac{\partial^3 u}{\partial z^3}-\begin{pmatrix}\frac{\partial u}{\partial x}\frac{\partial^2 u}{\partial z^2}+\frac{\partial u}{\partial z}\frac{\partial^2 w}{\partial z^2}\\ 2\frac{\partial u}{\partial z}\frac{\partial^2 u}{\partial x\partial z}+2\frac{\partial w}{\partial z}\frac{\partial^2 u}{\partial z^2}\end{pmatrix}\right), \tag{2}$$

$$u\frac{\partial v}{\partial x}+v\frac{\partial v}{\partial y}+w\frac{\partial v}{\partial z}=v\frac{\partial^2 v}{\partial z^2}-K\left(u\frac{\partial^3 v}{\partial x\partial z^2}+w\frac{\partial^3 v}{\partial z^3}-\begin{pmatrix}\frac{\partial v}{\partial x}\frac{\partial^2 v}{\partial z^2}+\frac{\partial v}{\partial z}\frac{\partial^2 w}{\partial z^2}\\ 2\frac{\partial v}{\partial z}\frac{\partial^2 v}{\partial x\partial z}+2\frac{\partial w}{\partial z}\frac{\partial^2 v}{\partial z^2}\end{pmatrix}\right), \tag{3}$$

$$u\frac{\partial T}{\partial x}+v\frac{\partial T}{\partial y}+w\frac{\partial T}{\partial z}=\alpha_m\frac{\partial^2 T}{\partial z^2}+\frac{D_B k_T}{C_s C_\rho}\frac{\partial^2 C}{\partial z^2}+\tau\left(D_B\frac{\partial C}{\partial z}\frac{\partial T}{\partial z}+\frac{D_T}{T_\infty}\left(\frac{\partial T}{\partial z}\right)^2\right), \tag{4}$$

$$u\frac{\partial C}{\partial x}+v\frac{\partial C}{\partial y}+w\frac{\partial C}{\partial z}=D_B\frac{\partial^2 C}{\partial z^2}-K_1(C-C_\infty)+\frac{Dk_T}{T_m}\frac{\partial^2 T}{\partial z^2}+\frac{D_T}{T_\infty}\frac{\partial^2 T}{\partial z^2}, \tag{5}$$

where u, v and w denote the velocity components in the x,y and $z$directions, respectively, $v=\frac{\mu}{\rho}$ the kinematic viscosity, K the material fluid parameter, C the concentration of the nanoparticles species, D_B the Brownian diffusion coefficients, K_1 the reaction rate, k_T the thermal diffusion, T the temperature, C_ρ the specific heat, C_s the concentration susceptibility, α_m the thermal diffusivity, and T_m the fluid mean temperature.

The boundary conditions for the present flow analysis can be written as

$$u=u_w(x)=ax,\quad v=v_w(y)=by,\quad w=0,$$
$$T=T_w,\quad C=C_w\quad \text{at } z=0, \tag{6}$$

$$u\to 0,\quad v\to 0,\quad \frac{\partial u}{\partial z}\to 0,\quad \frac{\partial v}{\partial z}\to y,\quad T\to T_\infty,$$
$$C\to C_\infty\quad \text{at } z\to\infty, \tag{7}$$

where C_w denotes the nanoparticles concentration at the surface, C_∞ is the nanoparticle concentration far away from the sheet, T_w is the surface temperature and T_∞ is the temperature far away from the surface. Using

$$\eta=\sqrt{\frac{a}{v}}z,\ u=axf'(\eta),\ v=ayg'(\eta),$$
$$w=-\sqrt{av}\{f(\eta)+g(\eta)\},\ \phi(\eta)=\frac{C-C_\infty}{C_w-C_\infty},\ \theta(\eta)=\frac{T-T_\infty}{T_w-T_\infty}. \tag{8}$$

Eq. (1) is identically satisfied while Eqs. (2)–(7) are reduced to

$$f'''-(f')^2+(f+g)f''+K_0\Big((f+g)f''''+(f''-g'')f''-2(f'+g')f'''\Big)=0, \tag{9}$$

$$g'''-(g')^2+(f+g)g''+K_0\big((f+g)g''''+(f''-g'')g''-2(f'+g')g'''\big)=0, \tag{10}$$

$$\theta''+\Pr((f+g)\theta'+(N_t\theta'+N_b\phi')\theta'+Du\phi'')=0, \tag{11}$$

$$\phi''+\Pr Le((f+g)\phi'-\gamma\phi+Sr\theta'')+\left(\frac{N_t}{N_b}\right)\theta''=0, \tag{12}$$

$$f(0)=0,\quad g(0)=0,\quad f'(0)=1,\quad g'(0)=c,$$
$$\theta(0)=1,\quad \phi(0)=1,$$
$$f'(\infty)\to 0,\quad f''(\infty)\to 0,\quad g'(\infty)\to 0,$$
$$g''(\infty)\to 0,\quad \theta(\infty)\to 0,\quad \phi(\infty)\to 0. \tag{13}$$

Please cite this article in press as: M. Ramzan et al., Three dimensional boundary layer flow of a viscoelastic nanofluid with Soret and Dufour effects, Alexandria Eng. J. (2015), http://dx.doi.org/10.1016/j.aej.2015.09.012

Here $K_0 = \frac{ka}{\nu}$ is the dimensionless viscoelastic parameter, prime is the differentiation with respect to η and the constant $a > 0$ and $b > 0$. Furthermore $Le$and Pr are the Lewis and Prandtl numbers, respectively, N_t and N_b are the Brownian motion and thermophoresis parameters respectively, γ is the chemical reaction parameter, Du is the Dufour number and Sr is the Soret number, which are defined below:

$$c=\frac{b}{a},\quad Le=\alpha/D_B,\quad \gamma=\frac{K_1}{a},\quad N_b=\frac{\tau D_B(C_w-C_\infty)}{\nu},\quad \Pr=\frac{\nu}{\alpha_m},$$
$$N_b=\frac{\tau D_T(T_w-T_\infty)}{\nu T_\infty},\quad Du=\frac{Dk_T}{C_sC_\rho}\frac{(C_w-C_\infty)}{(T_w-T_\infty)\nu},\quad Sr=\frac{Dk_T}{\nu T_m}\frac{(T_w-T_\infty)}{(C_w-C_\infty)}. \tag{14}$$

We point out that the two dimension ($g = 0$) case has been recovered for $c = 0$. For $c = 1$, we obtain axisymmetric case, i.e. ($f = g$). The Local Nusselt and Sherwood numbers are

$$Nu_x=-\frac{x\left(\frac{\partial T}{\partial z}\right)_{z=0}}{(T_w-T_\infty)},\quad Sh_x=-\frac{x\left(\frac{\partial C}{\partial z}\right)_{z=0}}{(C_w-C_\infty)}. \tag{15}$$

Dimensionless forms of local Nusselt and Sherwood numbers are as follows:

$$N_{u_x}\mathrm{Re}_x^{-1/2}=-\theta'(0),\quad Sh\mathrm{Re}_x^{-1/2}=-\phi'(0), \tag{16}$$

where $\mathrm{Re}_x = ux/\nu$ is the local Reynolds number.

3. Homotopic solutions

Homotopy analysis method requires initial guesses $(f_0, g_0, \theta_0, \phi_0)$ and linear operators $(\mathcal{L}_f, \mathcal{L}_g, \mathcal{L}_\theta, \mathcal{L}_\phi)$ in the forms

$$f_0(\eta)=1-\exp(-\eta),\quad g_0(\eta)=c(1-\exp(-\eta)),$$
$$\theta_0(\eta)=\exp(-\eta),\quad \phi_0(\eta)=\exp(-\eta). \tag{17}$$

The auxiliary linear operators are chosen as

$$\mathcal{L}_f(\eta)=\frac{d^3f}{d\eta^3}-\frac{df}{d\eta},\quad \mathcal{L}_g(\eta)=\frac{d^3g}{d\eta^3}-\frac{dg}{d\eta},$$
$$\mathcal{L}_\theta(\eta)=\frac{d^2\theta}{d\eta^2}-\theta,\quad \mathcal{L}_\phi(\eta)=\frac{d^2\phi}{d\eta^2}-\phi. \tag{18}$$

The auxiliary linear operators have the following properties:

$$\mathcal{L}_f[C_1+C_2\exp(\eta)+C_3\exp(-\eta)]=0, \tag{19}$$
$$\mathcal{L}_g[C_4+C_5\exp(\eta)+C_6\exp(-\eta)]=0, \tag{20}$$
$$\mathcal{L}_\theta[C_7\exp(\eta)+C_8\exp(-\eta)]=0, \tag{21}$$
$$\mathcal{L}_\phi[C_9\exp(\eta)+C_{10}\exp(-\eta)]=0, \tag{22}$$

where C_i $(i = 1 - 10)$ are the arbitrary constants. The zeroth and mth order deformation problems are stated below.

3.1. Zeroth-order deformation problems

$$(1-p)\mathcal{L}_f\left[\widehat{f}(\eta;p)-f_0(\eta)\right]=p\hbar_f\mathcal{N}_f\left[\widehat{f}(\eta;p),\widehat{g}(\eta;p)\right], \tag{23}$$

$$(1-p)\mathcal{L}_g[\widehat{g}(\eta;p)-g_0(\eta)]=p\hbar_g\mathcal{N}_g\left[\widehat{f}(\eta;p),\widehat{g}(\eta;p)\right], \tag{24}$$

$$(1-p)\mathcal{L}_\theta\left[\widehat{\theta}(\eta;p)-\theta_0(\eta)\right]=p\hbar_\theta\mathcal{N}_\theta\left[\widehat{f}(\eta;p),\widehat{g}(\eta;p),\widehat{\theta}(\eta;p),\widehat{\phi}(\eta;p)\right], \tag{25}$$

$$(1-p)\mathcal{L}_\phi\left[\widehat{\phi}(\eta;p)-\phi_0(\eta)\right]=p\hbar_\phi\mathcal{N}_\phi\left[\widehat{f}(\eta;p),\widehat{g}(\eta;p),\widehat{\theta}(\eta;p),\widehat{\phi}(\eta;p)\right], \tag{26}$$

$$\widehat{f}(\eta;p)\Big|_{\eta=0}=0,\quad \frac{\partial\widehat{f}(\eta;p)}{\partial\eta}\Big|_{\eta=0}=1,$$
$$\frac{\partial\widehat{f}(\eta;p)}{\partial\eta}\Big|_{\eta=\infty}=0,\quad \frac{\partial^2\widehat{f}(\eta;p)}{\partial\eta^2}\Big|_{\eta=\infty}=0, \tag{27}$$

$$\widehat{g}(\eta;p)|_{\eta=0}=0,\quad \frac{\partial\widehat{g}(\eta;p)}{\partial\eta}\Big|_{\eta=0}=c,$$
$$\frac{\partial\widehat{g}(\eta;p)}{\partial\eta}\Big|_{\eta=\infty}=0,\quad \frac{\partial^2\widehat{g}(\eta;p)}{\partial\eta^2}\Big|_{\eta=\infty}=0, \tag{28}$$

$$\widehat{\theta}(\eta;p)\Big|_{\eta=0}=1,\quad \widehat{\theta}(\eta;p)\Big|_{\eta=\infty}=0, \tag{29}$$

$$\widehat{\phi}(\eta;p)\Big|_{\eta=0}=1,\quad \widehat{\phi}(\eta;p)\Big|_{\eta=\infty}=0. \tag{30}$$

$$\mathcal{N}_f\left[\widehat{f}(\eta,p),\widehat{g}(\eta;p)\right]=\frac{\partial^3\widehat{f}(\eta;p)}{\partial\eta^3}-\left(\frac{\partial\widehat{f}(\eta;p)}{\partial\eta}\right)^2$$
$$+\left\{\widehat{f}(\eta;p)+\widehat{g}(\eta;p)\right\}\frac{\partial^2\widehat{f}(\eta;p)}{\partial\eta^2}K_0\begin{bmatrix}\left\{\widehat{f}(\eta;p)+\widehat{g}(\eta;p)\right\}\widehat{f}'''(\eta;p)\\+\left\{\widehat{f}'(\eta;p)+\widehat{g}''(\eta;p)\right\}\widehat{f}''(\eta;p)\\-2\left\{\widehat{f}'(\eta;p)+\widehat{g}'(\eta;p)\right\}\widehat{f}'''(\eta;p)\end{bmatrix}, \tag{31}$$

$$\mathcal{N}_g\left[\widehat{f}(\eta,p),\widehat{g}(\eta,p)\right]=\frac{\partial^3\widehat{g}(\eta;p)}{\partial\eta^3}-\left(\frac{\partial\widehat{g}(\eta;p)}{\partial\eta}\right)^2$$
$$+\left\{\widehat{f}(\eta;p)+\widehat{g}(\eta;p)\right\}\frac{\partial^2\widehat{g}(\eta;p)}{\partial\eta^2}K_0\begin{bmatrix}\left\{\widehat{f}(\eta;p)+\widehat{g}(\eta;p)\right\}\widehat{g}'''(\eta;p)\\+\left\{\widehat{f}''(\eta;p)+\widehat{g}''(\eta;p)\right\}\widehat{g}''(\eta;p)\\-2\left\{\widehat{f}'(\eta;p)+\widehat{g}'(\eta;p)\right\}\widehat{g}'''(\eta;p)\end{bmatrix}, \tag{32}$$

$$\mathcal{N}_\theta\left[\widehat{f}(\eta;p),\widehat{g}(\eta;p),\widehat{\theta}(\eta,p),\widehat{\phi}(\eta;p)\right]$$
$$=\frac{\partial^2\widehat{\theta}(\eta,p)}{\partial\eta^2}+\Pr\begin{Bmatrix}\left(\widehat{f}(\eta;p)+\widehat{g}(\eta;p)\right)\frac{\partial\widehat{\theta}(\eta;p)}{\partial\eta}\\-\left(N_b\frac{\partial\widehat{\phi}(\eta;p)}{\partial\eta}+N_t\frac{\partial\widehat{\theta}(\eta;p)}{\partial\eta}\right)\frac{\partial\widehat{\theta}(\eta;p)}{\partial\eta}\\+Du\frac{\partial^2\widehat{\phi}(\eta,p)}{\partial\eta^2}\end{Bmatrix}, \tag{33}$$

$$\mathcal{N}_\phi\left[\widehat{f}(\eta;p),\widehat{g}(\eta,p),\widehat{\theta}(\eta;p),\widehat{\phi}(\eta;p)\right]$$
$$=\frac{\partial^2\widehat{\phi}(\eta,p)}{\partial\eta^2}+\mathrm{PrLe}\begin{Bmatrix}\left(\widehat{f}(\eta;p)+\widehat{g}(\eta;p)\right)\frac{\partial\widehat{\phi}(\eta;p)}{\partial\eta}\\-\gamma\widehat{\phi}(\eta;p)+Sr\frac{\partial^2\widehat{\theta}(\eta,p)}{\partial\eta^2}\end{Bmatrix}$$
$$+\left(\frac{N_t}{N_b}\right)\frac{\partial^2\widehat{\theta}(\eta,p)}{\partial\eta^2}. \tag{34}$$

For $p = 0$ and $p = 1$, we have

$$\widehat{f}(\eta;0)=f_0(\eta),\quad \widehat{f}(\eta;1)=f(\eta), \tag{35}$$

$$\widehat{g}(\eta;0)=g_0(\eta),\quad \widehat{g}(\eta;1)=g(\eta), \tag{36}$$

$$\widehat{\theta}(\eta;0)=\theta_0(\eta),\quad \widehat{\theta}(\eta;1)=\theta(\eta), \tag{37}$$

$$\widehat{\phi}(\eta;0)=\phi_0(\eta),\quad \widehat{\phi}(\eta;1)=\phi(\eta), \tag{38}$$

and when p increases from 0 to 1, $\widehat{f}(\eta;p),\widehat{g}(\eta;p),\widehat{\theta}(\eta;p)$ and $\widehat{\phi}(\eta;p)$ deform from $g_0(\eta),f_0(\eta),\theta_0(\eta)$ and $\phi_0(\eta)$ to $f(\eta),g(\eta),\theta(\eta)$ and $\phi(\eta)$, respectively. Expanding $\widehat{f}(\eta;p),\widehat{g}(\eta;p),\widehat{\theta}(\eta;p)$ and $\widehat{\phi}(\eta;p)$, we have

$$\widehat{f}(\eta;p)=f_0(\eta)+\sum_{m=1}^{\infty}f_m(\eta)p^m, \tag{39}$$

$$\widehat{g}(\eta;p)=g_0(\eta)+\sum_{m=1}^{\infty}g_m(\eta)p^m, \tag{40}$$

$$\widehat{\theta}(\eta;p)=\theta_0(\eta)+\sum_{m=1}^{\infty}\theta_m(\eta)p^m, \tag{41}$$

$$\widehat{\phi}(\eta;p)=\phi_0(\eta)+\sum_{m=1}^{\infty}\phi(\eta)p^m. \tag{42}$$

3.2. mth-order deformation problems

The subjected problems at the mth order are given by

$$\mathcal{L}_f[f_m(\eta)-\chi_m f_{m-1}(\eta)]=\hbar_f\mathcal{R}_m^f(\eta), \tag{43}$$

$$\mathcal{L}g[g_m(\eta)-\chi_m g_{m-1}(\eta)]=\hbar_g\mathcal{R}_m^g(\eta), \tag{44}$$

$$\mathcal{L}_\theta[\theta_m(\eta)-\chi_m\theta_{m-1}(\eta)]=\hbar_\theta\mathcal{R}_m^\theta(\eta), \tag{45}$$

$$\mathcal{L}_\phi[\phi_m(\eta)-\chi_m\phi_{m-1}(\eta)]=\hbar_\phi\mathcal{R}_m^\phi(\eta), \tag{46}$$

$$f_m(0)=f_m'(0)=f_m'(\infty)=f_m''(\infty)=0, \tag{47}$$

$$g_m(0)=g_m'(0)=g_m'(\infty)=g_m''(\infty)=0, \tag{48}$$

$$\theta_m(0)=\theta_m(\infty)=0, \tag{49}$$

$$\phi_m(0)=\phi_m(\infty)=0, \tag{50}$$

$$\mathcal{R}_m^f(\eta)=f_{m-1}'''+\sum_{k=0}^{m-1}\left[\begin{array}{c}(f_{m-1-k}+g_{m-1-k})f_k''-f_{m-1-k}'f_k'\\ +K_0\left\{\begin{array}{c}(f_{m-1-k}+g_{m-1-k})f_k^{iv}\\ +(f_{m-1-k}''-g_{m-1-k}'')f_k''\\ -2(f_{m-1-k}'-g_{m-1-k}')f_k'''\end{array}\right\}\end{array}\right], \tag{51}$$

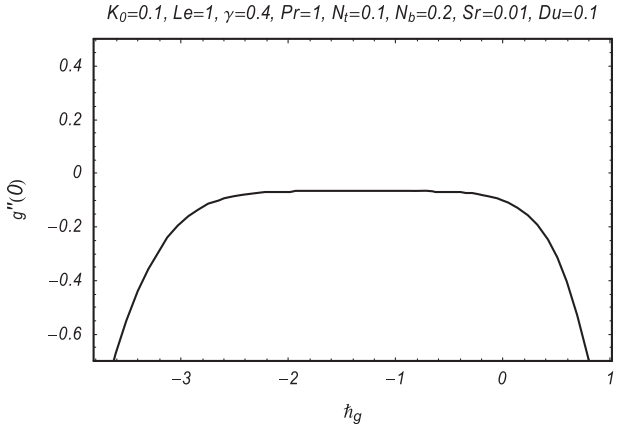

Figure 2 $\hbar$ curve of g.

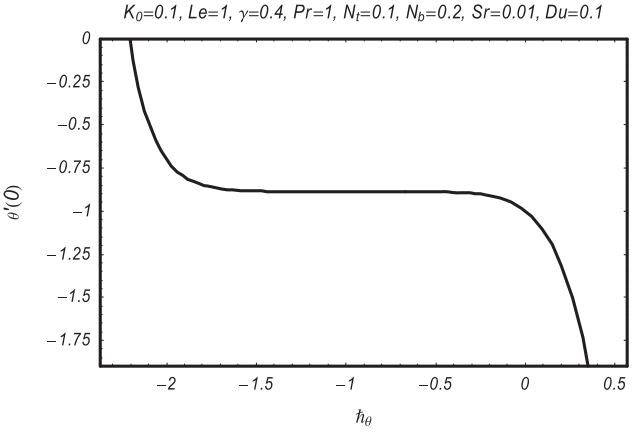

Figure 3 $\hbar$ curve of θ.

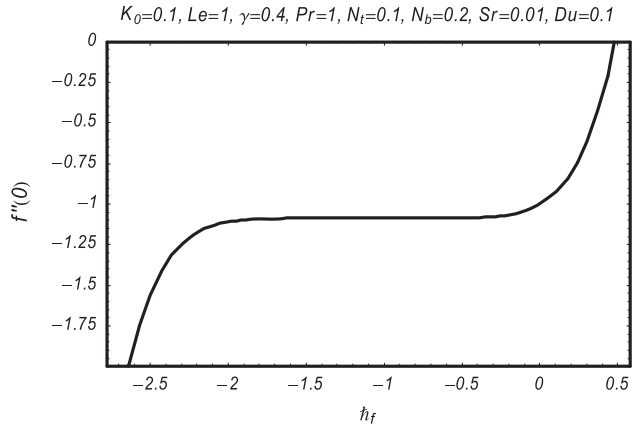

Figure 1 $\hbar$ curve of f.

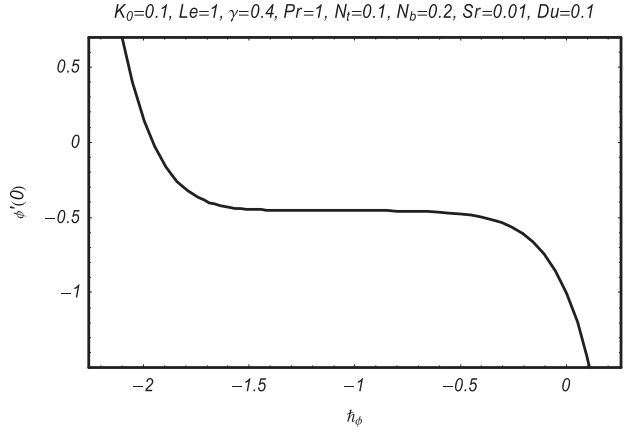

Figure 4 $\hbar$ curve of ϕ.

Table 1 Convergence of series solutions for different order of approximations when $K_0 = 0.1, Du = 0.1, \gamma = 0.4, \Pr = 1, N_t = 0.1, c = 0.1, Le = 1, N_b = 0.2$, and $Sr = 0.01$.

Order of approximations	$-f''(0)$	$-g''(0)$	$-\theta'(0)$	$-\phi'(0)$
1	1.0627	0.082267	0.62667	0.90533
4	1.0869	0.068139	0.47381	0.88210
6	1.0875	0.066931	0.45356	0.88899
10	1.0877	0.066640	0.45406	0.88901
12	1.0877	0.066613	0.45287	0.88901
25	1.0877	0.066611	0.45111	0.88901
30	1.0877	0.066611	0.45111	0.88901

$$\mathcal{R}^g_m(\eta) = g'''_{m-1} + \sum_{k=0}^{m-1}\left[\begin{array}{l}(f_{m-1-k}+g_{m-1-k})g''_k - g'_{m-1-k}g'_k \\ +K_0\left\{\begin{array}{l}(f_{m-1-k}+g_{m-1-k})g^{iv}_k \\ +(f''_{m-1-k}-g''_{m-1-k})g''_k \\ -2(f'_{m-1-k}-g'_{m-1-k})g'''_k\end{array}\right\}\end{array}\right], \quad (52)$$

$$\mathcal{R}^\theta_m(\eta) = \theta''_{m-1} + \Pr\sum_{k=0}^{m-1}(f_{m-1-k}\theta'_k + g_{m-1-k}\theta'_k)\Pr\left(N_b\sum_{k=0}^{m-1}\phi'_{m-1-k}\theta'_k + N_t\sum_{k=0}^{m-1}\theta'_{m-1-k}\theta'_k\right) + \Pr Du\sum_{k=0}^{m-1}\phi''_{m-1}, \quad (53)$$

$$\mathcal{R}^\phi_m(\eta) = \phi''_{m-1} - \Pr Le\gamma\phi_{m-1} + \Pr Le\sum_{k=0}^{m-1}(f_{m-1-k}\phi'_k - g_{m-1-k}\phi'_k) + \Pr LeSr\theta''_{m-1} + \frac{N_t}{N_b}\theta''_{m-1} \quad (54)$$

$$\chi_m = \begin{cases}0, m \leqslant 1\\ 1, m > 1\end{cases}. \quad (55)$$

The final solutions can be written in the following forms:

$$f_m(\eta) = f^\star_m(\eta) + A_1 + A_2e^\eta + A_3e^{-\eta}, \quad (56)$$

$$g_m(\eta) = g^\star_m(\eta) + A_4 + A_5e^\eta + A_6e^{-\eta}, \quad (57)$$

$$\theta_m(\eta) = \theta^\star_m(\eta) + A_7e^\eta + A_8e^{-\eta}, \quad (58)$$

$$\phi_m(\eta) = \phi^\star_m(\eta) + A_9e^\eta + A_{10}e^{-\eta}, \quad (59)$$

where $f^*_m, g^*_m, \theta^*_m,$ *and* ϕ^*_m denote the special solution.

4. Convergence analysis

To find the meaningful series solutions of velocities, temperature and nanoparticle concentration equations, the convergence region is essential to determine. Convergence region of the series solutions depends upon the auxiliary parameter $\hbar$. Therefore we have plotted the $\hbar$-curves in Figs. 1–4. The appropriate ranges of the auxiliary parameters $\hbar_f, \hbar_g, \hbar_\theta$ and $\hbar_\phi$ are $-2 \leqslant \hbar_f \leqslant -0.4, -2 \leqslant \hbar_g \leqslant -0.7, -1.5 \leqslant \hbar_\theta \leqslant -0.8$ and $-1.5 \leqslant \hbar_\phi \leqslant -0.4$.

5. Results and discussion

The basic theme of this section is to examine the influences of physical parameters on the physical quantities, dimensionless velocities, temperature and nanoparticles concentration. Table 1 gives the numerical values of $f''(0), g''(0), \theta'(0)$ and $\phi'(0)$ at different order of HAM approximations. Here we noted that the values of $f''(0)$ and $\phi'(0)$ converge from 10-th order of approximations while the values of $g''(0)$ and $\theta'(0)$ converge from 25-th order of HAM deformations. Here we

Table 2 Numerical values of Sherwood number $Sh_x/\mathrm{Re}_x^{1/2}$ and Nusselt number $Nu_x/\mathrm{Re}_x^{1/2}$ for different parameters.

K_0	Du	γ	Pr	N_t	c	Le	N_b	Sr	$-\theta'(0)$	$-\phi'(0)$
0.1	0.1	0.4	1	0.1	0.1	1	0.2	0.01	0.45100	0.88901
0.2									0.44000	0.88150
0.3									0.42536	0.87271
	0.2								0.39300	0.88881
	0.3								0.33463	0.88859
		0.3							0.45960	0.82776
		0.4							0.45100	0.88901
		0.5							0.44714	0.94594
			0.9						0.43348	0.83822
			1						0.45100	0.88901
			1.1						0.47008	0.93739
				0.2					0.43111	0.88569
				1					0.30061	0.84119
					0.2				0.47805	0.91000
					0.3				0.50061	0.92967
						0.9			0.45846	0.83819
						1			0.45100	0.88901
						1.1			0.44764	0.93743
							0.1		0.48290	0.88631
							0.2		0.45100	0.88901
							0.3		0.42483	0.88990
								0.01	0.45100	0.88901
								0.02	0.45341	0.88601
								0.99	0.48293	0.59573

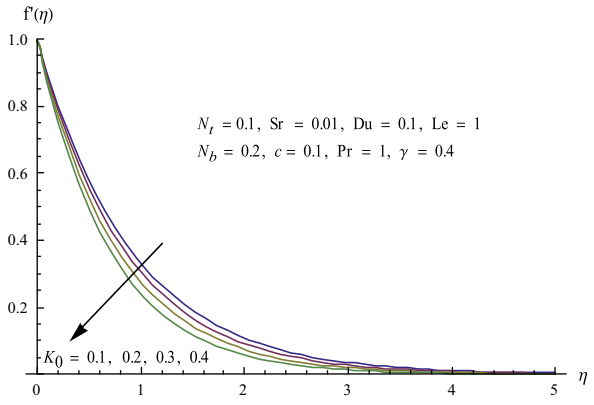

Figure 5 Influence of K_0 on f'.

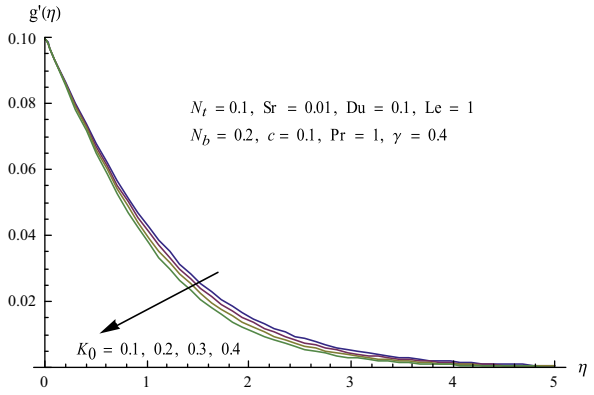

Figure 6 Influence of K_0 on g'.

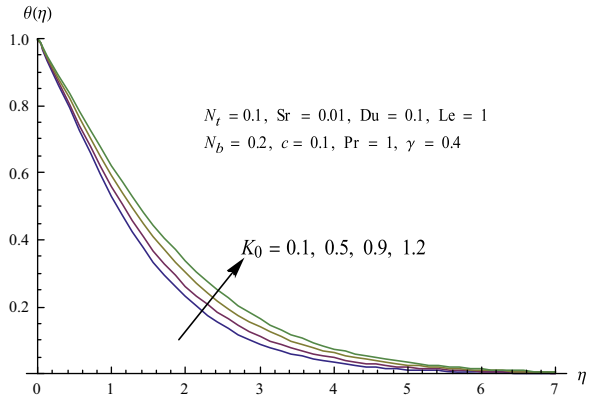

Figure 7 Influence of K_0 on θ.

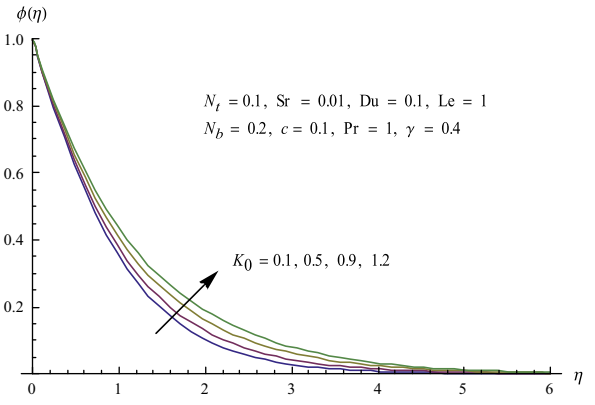

Figure 8 Influence of K_0 on ϕ.

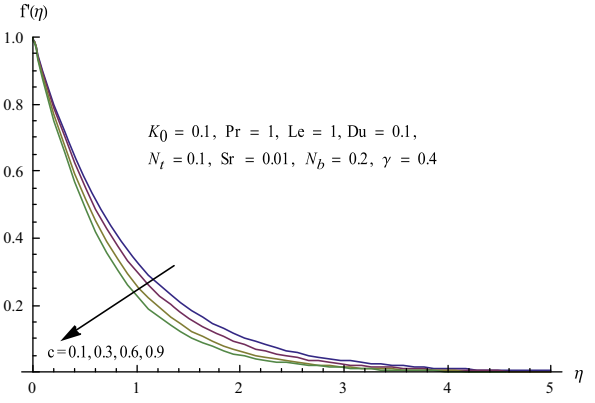

Figure 9 Influence of c on f'.

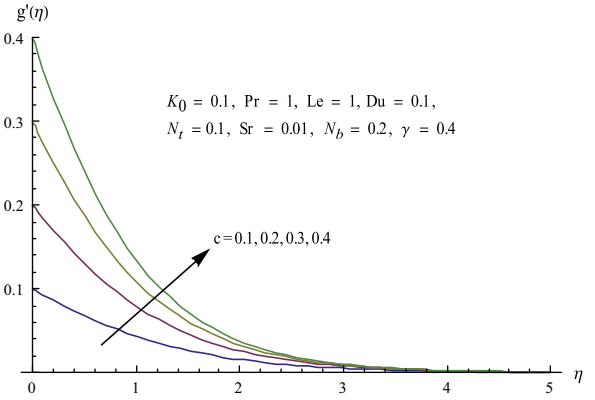

Figure 10 Influence of c on g'.

concluded that 25-th order HAM deformations are essential for the convergent solutions. Table 2 shows the numerical values of local Nusselt number $-\theta'(0)$ and local Sherwood number $-\phi'(0)$ for various values of $K_0, Du, \gamma, \mathrm{Pr}, N_t, c, Le, N_b$ and Sr. We noted that the values of local Nusselt and Sherwood numbers are decreased with an increase in K_0, Du and N_t while these values are enhanced for the larger values of Pr and c.

Figs. 5 and 6 show the behaviors of K_0 on the dimensionless velocities field $f'(\eta)$ and $g'(\eta)$. From these figures we examine that the velocities $f'(\eta)$ and $g'(\eta)$ are decreased for the increasing values of K_0. An increase in K_0 leads to stronger viscoelasticity which resists the fluid flow due to which the fluid velocities are reduced. The influence of K_0 on the temperature $\theta(\eta)$ and nanoparticles concentration $\phi(\eta)$ is studied in Figs. 7 and 8. It is seen that both the temperature and nanoparticle concentration are enhanced when we increase the values of K_0. From Figs. 9 and 10, we observed that the velocity $f'(\eta)$

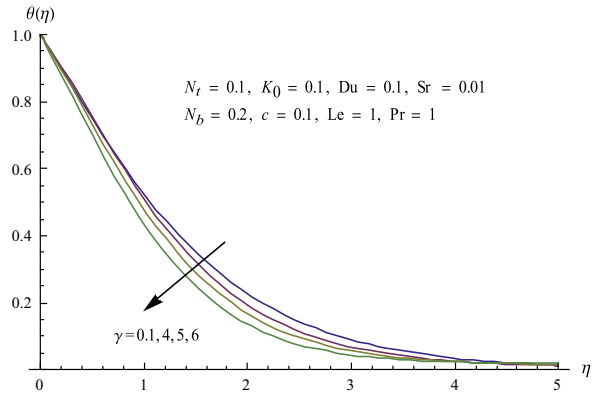

Figure 11 Influence of γ on θ.

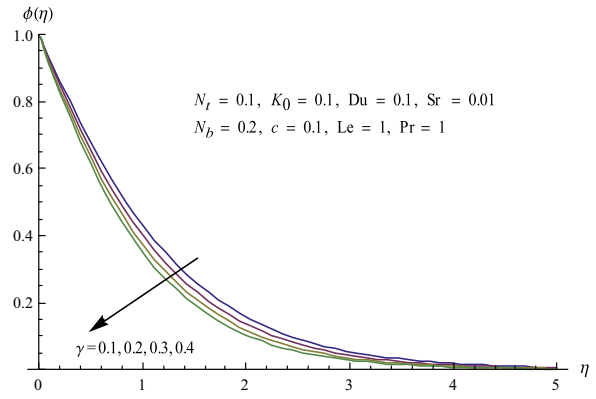

Figure 12 Influence of γ on ϕ.

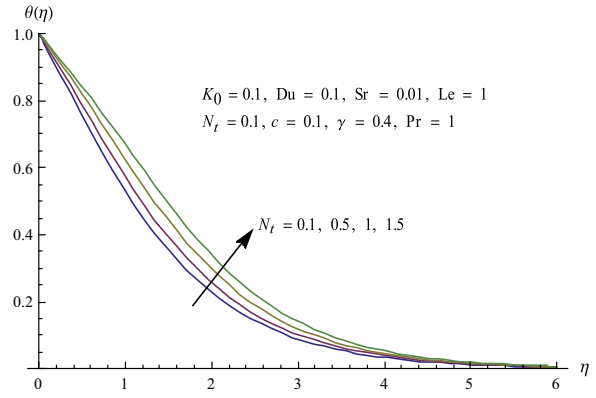

Figure 13 Influence of N_t on θ.

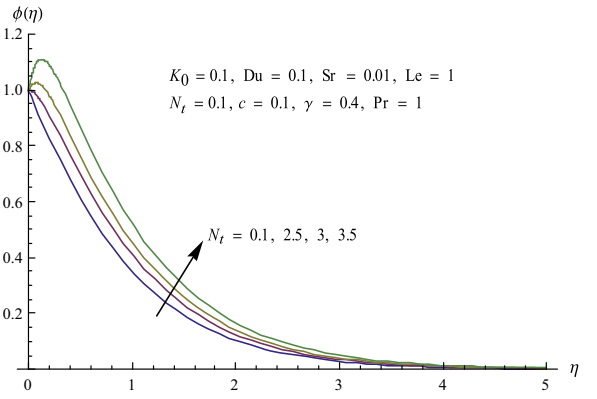

Figure 14 Influence of N_t on ϕ.

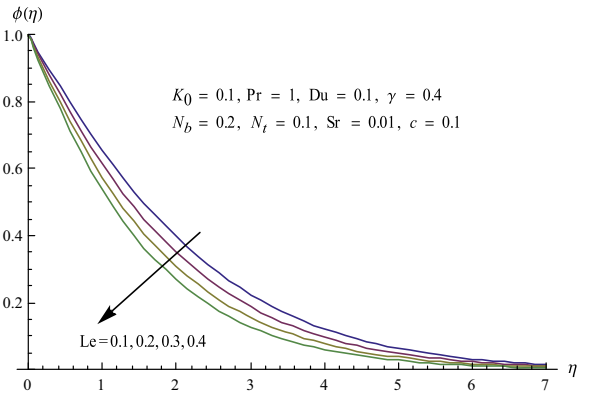

Figure 15 Influence of Le on ϕ.

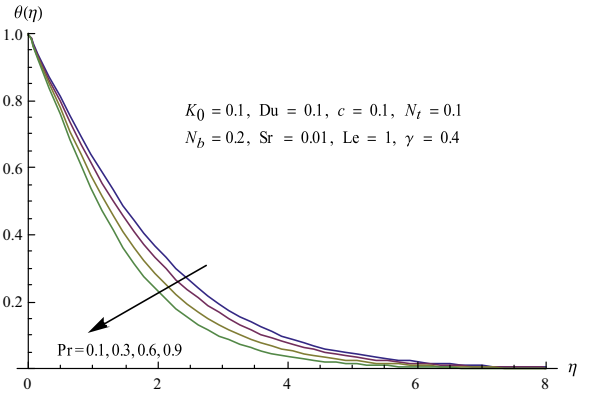

Figure 16 Influence of Pr on θ.

is decreased while the velocity $g'(\eta)$ is increased with an increase in the ratio parameter c.

The effects of chemical reaction parameter γ on the temperature and nanoparticle concentration are analyzed in Figs. 11 and 12. We have seen that the temperature, nanoparticle concentration and their associated boundary layer thicknesses are decreasing functions of chemical reaction parameters. Figs. 13 and 14 are stretched to examine the change in the temperature and nanoparticle concentration corresponding to different values of thermophoresis parameter N_t. The larger values of thermophoresis parameter lead to an enhancement in thermal and nanoparticle concentration boundary layer thicknesses. Fig. 15 presents that the larger values of Lewis number Le correspond to a reduction in the nanoparticles concentration. Here the Lewis number is inversely proportional to the Brownian diffusion coefficient. Larger Lewis number implies to weaker Brownian diffusion coefficient due to which the nanoparticle concentration is decreased. The variations in

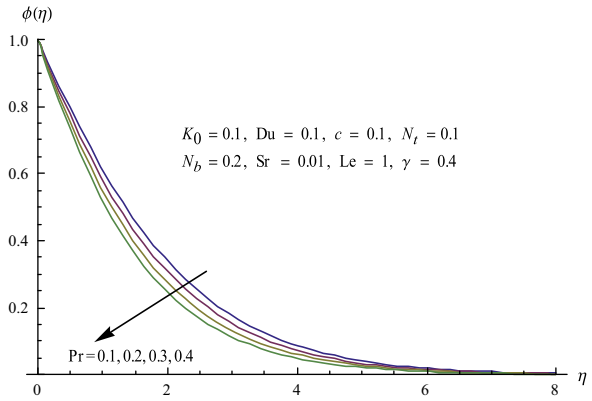

Figure 17 Influence of Pr on ϕ.

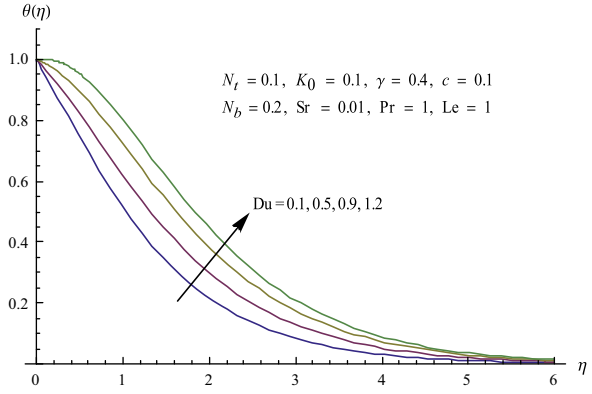

Figure 18 Influence of Du on θ.

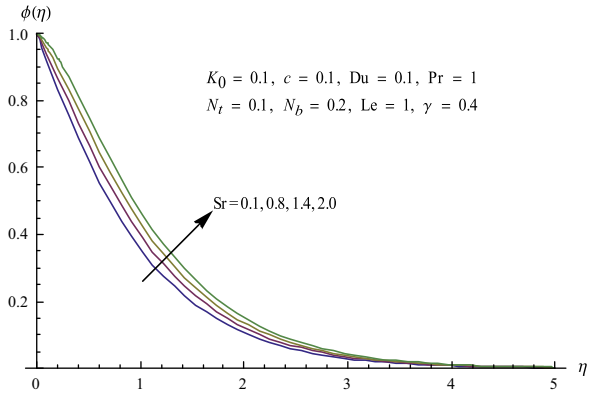

Figure 19 Influence of Sr on ϕ.

the temperature and nanoparticle concentration for different values of Prandtl number Pr are examined in Figs. 16 and 17. An increase in Prandtl number leads to the reduction in the temperature and nanoparticle concentration. Prandtl number is strongly dependent on thermal diffusivity of fluid. Larger Prandtl number fluid has weaker thermal diffusivity. Such weaker thermal diffusivity is responsible for a reduction in temperature and nanoparticle concentration. Figs. 18 and 19 clearly show that the effect of Dufour and Soret numbers

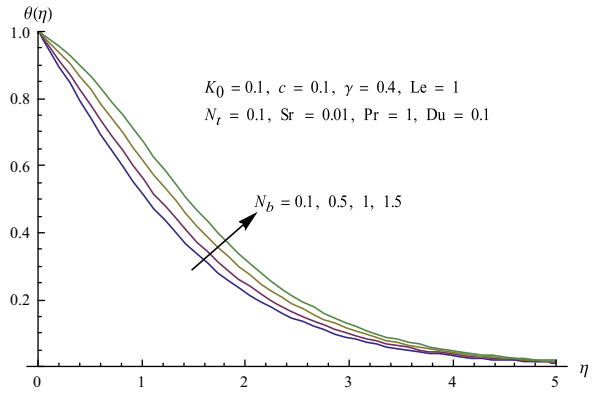

Figure 20 Influence of N_b on θ.

on both the temperature and nanoparticle concentration is similar. Here temperature and nanoparticle concentration are increasing functions of Du and Sr. From Fig. 20, one can see that the temperature is enhanced when we increase the values of Brownian motion parameter N_b.

6. Conclusion

We started the three-dimensional boundary layer flow of viscoelastic fluid under Soret-Dufour and nanoparticles effects over a stretching surface. The main points of this investigation are as follows:

- The convergent series solutions are obtained by computing 25-th order HAM deformations.
- The values of local Nusselt and Sherwood numbers are quite reverse for the increasing values of Le and Sr.
- Temperature and nanoparticles concentration are enhanced with an increase in thermophoresis parameter.
- Nanoparticle concentration field is a decreasing function of Lewis number Le.
- An increase in Dufour number gives rise to the temperature and thermal boundary layer thickness.
- Temperature field is enhanced for the larger Brownian motion parameter.

Acknowledgement

This project is funded by the Deanship of Scientific Research (DSR), Majmaah University, Saudi Arabia. The author therefore acknowledges with thanks DSR for technical and financial support.

References

[1] S.U.S. Choi, Enhancing thermal conductivity of fluids with nanoparticles, in: Proceeding of ASME International Mechanical Engineering Congress and Exposition, vol. 66, San Francisco, Calif, USA, 1995, pp. 99–105.
[2] K. Kwak, C. Kim, Viscosity and thermal conductivity of copper oxide nanofluid dispersed in ethylene glycol, Korea–Australia Rheol. J. 17 (2) (2005) 35–40.
[3] M. Ramzan, Influence of Newtonian heating on three dimensional MHD flow of couple stress nanofluid with viscous

dissipation and joule heating, PLoS ONE 10 (4) (2015) e0124699, http://dx.doi.org/10.1371/journal.pone.0124699.
[4] M. Turkyilmazoglu, I. Pop, Heat and mass transfer of unsteady natural convection flow of some nanofluids past a vertical infinite flat plate with radiation effect, Int. J. Heat Mass Transfer 59 (2013) 167–171.
[5] M. Sheikholeslami, M. Gorji-Bandpy, D.D. Ganji, MHD free convection in an eccentric semi-annulus filled with nanofluid, J. Taiwan Inst. Chem. Eng. 45 (4) (2014) 1204–1216.
[6] M. Sheikholeslami, D.D. Ganji, Three dimensional heat and mass transfer in rotating system using nanofluid, Powder Technol. 253 (2014) 789–796.
[7] M.M. Rashidi, S. Abelman, N. Freidooni Mehr, Entropy generation in steady MHD flow due to a rotating porous disk in a nanofluid, Int. J. Heat Mass Transfer 62 (2013) 515–525.
[8] M. Ramzan, M. Bilal, Time dependent MHD nano-second grade fluid flow induced by permeable vertical sheet with mixed convection and thermal radiation, PLoS ONE 10 (5) (2015) e0124929, http://dx.doi.org/10.1371/journal.pone.0124929.
[9] S. Khamis, O.D. Makinde, Y.N. Gyekye, Modelling the effects of variable viscosity in unsteady flow of nanofluids in a pipe with permeable wall and convective cooling, Appl. Comput. Math. 3 (3) (2014) 75–84.
[10] T. Hussain, S.A. Shehzad, A. Alsaedi, T. Hayat, M. Ramzan, Flow of Casson nanofluid with viscous dissipation and convective conditions: a mathematical model, J. Central South Univ. 22 (2015) 1132–1140.
[11] M. Imtiaz, T. Hayat, M. Hussain, S.A. Shehzad, G.Q. Chen, B. Ahmad, Mixed convection flow of nanofluid with newtonian heating, Eur. Phys. J. Plus 129 (5) (2014), http://dx.doi.org/10.1140/epjp/i2014-14097-y.
[12] M. Ramzan, F. Yousaf, Boundary layer flow of three-dimensional viscoelastic nanofluid past a bi-directional stretching sheet with Newtonian heating, AIP Adv. 5 (2015) 057132, http://dx.doi.org/10.1063/1.4921312.
[13] C.Y. Wang, The three-dimensional flow due to a stretching flat surface, Phys. Fluids 27 (8) (1984) 1915.
[14] P.D. Ariel, The three-dimensional flow past a stretching sheet and the homotopy perturbation method, Comput. Math. Appl. 54 (7–8) (2007) 920–925.
[15] T. Hayat, S.A. Shehzad, A. Alsaedi, M.S. Alhothuali, Three-dimensional flow of Oldroyd-B fluid over surface with convective boundary conditions, Appl. Math. Mech. 34 (4) (2013) 489–500.
[16] S.A. Shehzad, A. Alsaedi, T. Hayat, Hydromagnetic steady flow of Maxwell fluid over a bidirectional stretching surface with prescribed surface temperature and prescribed surface heat flux, PLoS ONE 8 (7) (2013) e68139.
[17] I. Ahmad, M. Ahmad, A. Abbas, M. Sajid, Hydromagnetic flow and heat transfer over a bidirectional stretching surface in a porous medium, Therm. Sci. 15 (2011) S205–S220.
[18] M. Turkyilmazoglu, Three dimensional MHD flow and heat transfer over a stretching/shrinking surface in a viscoelastic fluid with various physical effects, Int. J. Heat Mass Transfer 78 (2014) 150–155.
[19] M. Turkyilmazoglu, The analytical solution of mixed convection heat transfer and fluid flow of a MHD viscoelastic fluid over a permeable stretching surface, Int. J. Mech. Sci. 77 (2013) 263–268.
[20] M. Turkyilmazoglu, Multiple solutions of heat and mass transfer of MHD slip flow for the viscoelastic fluid over a stretching sheet, Int. J. Therm. Sci. 50 (11) (2011) 2264–2276.
[21] E.R.G. Eckert, R.M. Drake, Analysis of Heat and Mass Transfer, McGraw Hill, New York, NY, USA, 1972.
[22] M. Turkyilmazoglu, I. Pop, Soret and heat effects on the unsteady radiative MHD free convective flow from an impulsive started infinite vertical plate, Int. J. Heat Mass Transfer 55 (25–26) (2012) 7635–7644.
[23] M.M. Rashidi, T. Hayat, E. Erfani, S.A.M. Pour, A.A. Hendi, Simultaneous effects of partial slip and thermal-diffusion and diffusion thermo on steady MHD convective flow due to a rotating disk, Commun. Nonlinear Sci. Numer. Simul. 16 (11) (2011) 4303–4317.
[24] F.E. Alsaedi, S.A. Shehzad, T. Hayat, S.J. Monaquel, Soret and Dufour effects on the unsteady mixed convection flow over a stretchin surface, J. Mech. 29 (2013) 623–632.
[25] S.A. Shehzad, F.E. Alsaedi, S.J. Monaquel, T. Hayat, Soret and Dufour effects on the stagnation point flow of Jeffery fluid with convective boundary conditions, Eur. Phys. J. Plus 128 (6) (2013), http://dx.doi.org/10.1140/epjp/i2013-13056-6.
[26] S.J. Liao, On the homotopy analysis method for nonlinear problems, Appl. Math. Comput. 147 (2004) 499–513.
[27] M. Turkyilmazoglu, A note on homotopy analysis method, Appl. Math. Lett. 23 (10) (2010) 1226–1230.
[28] M.M. Rashidi, M. Ali, N. Friedoonimehr, F. Nazir, Parameteric analysis and optimization of entropy generation in unsteady MHD flow over a stretching rotation disk using artificial neural network and particle swarm optimization algorithm, Energy 55 (2013) 497–510.
[29] M. Ramzan, M. Farooq, A. Alsaedi, T. Hayat, MHD three dimensional flow of couple stress fluid with, Eur. Phys. J. Plus 128 (5) (2013) 49–63.
[30] S. Abbasbandy, T. Hayat, A. Alsaedi, M.M. Rashidi, Numerical and analytical solutions for Falkner-Skan flow of MHD Oldryod B-fluid, Int. J. Numer. Methods Heat Fluid Flow 24 (2) (2014) 390–401.
[31] S.A. Shehzad, T. Hayat, M.S. Alhuthali, S. Asghar, MHD three-dimensional flow of Jeffery fluid with Newtonian heat, J. Central South Univ. Technol. 21 (4) (2014) 1428–1433.
[32] T. Hayat, S.A. Shehzad, A. Alsaedi, Three-dimensional flow of Jeffery fluid over a bidirectional stretching surface with heat source/sink, J. Aerospace Eng. 27 (2014) 04014007.
[33] T. Hayat, S. Asad, A. Alsaedi, Flow of variable thermal conductivity fluid due to inclined stretching cylinder with viscous dissipation and thermal radiation, Appl. Math. Mech. 35 (2014) 717–728.

Please cite this article in press as: M. Ramzan et al., Three dimensional boundary layer flow of a viscoelastic nanofluid with Soret and Dufour effects, Alexandria Eng. J. (2015), http://dx.doi.org/10.1016/j.aej.2015.09.012